2018 European Control Conference (ECC)
June 12-15, 2018. Limassol, Cyprus

An Interval Observer Approach for the Online Temperature Estimation in Solid Oxide Fuel Cell Stacks

Andreas Rauh, Julia Kersten, and Harald Aschemann[1]

Abstract— **Interval observers that are based on the structural property of cooperativity allow for the computation of guaranteed lower and upper bounds for all state trajectories of dynamic systems by defining two sets of bounding systems for the dynamic behavior. In such a way, they remove the disadvantage of predictor–corrector interval estimation schemes which often suffer from the fact that the dynamic system model has to be evaluated over finitely large domains of state variables and parameters (often interval boxes or zonotopes). This evaluation typically results in overestimation that includes unphysical parts of the state-space in the computed results. To counteract this so-called wrapping effect, computationally expensive, problem-specific algorithms need to be implemented. However, this drawback can be removed for systems that have certain monotonicity and stability properties. In this paper, it is shown that appropriately defined system models for the thermal behavior of high-temperature fuel cells belong to this class of systems. The corresponding interval observer design is presented methodologically and demonstrated with the help of measured data from a test rig available at the Chair of Mechatronics at the University of Rostock.**

I. Introduction

Solid oxide fuel cells (SOFCs), operating at high temperature levels, provide the possibility to generate thermal and electrical energy in a decentralized fashion directly from the chemical energy contained in a fuel gas. In contrast to low-temperature fuel cells, SOFCs are more flexible with respect to the fuel gas that can be used. Besides hydrogen, also mixtures with methane, carbon dioxide, or carbon monoxide are possible due to the internal gas reforming capabilities of SOFCs. Due to the fact that the chemical energy included in the supplied gas is not converted by a classical combustion process, the efficiency of SOFCs is theoretically not restricted by the Carnot efficiency [1]–[4].

Despite these advantageous properties, SOFCs show nonlinear dynamics if variations of both the thermal and electrical operating points are desired. Moreover, it is necessary that the internal temperature of the SOFC stack (often constructed as an electric series connection of multiple planar fuel cells) does not exceed certain threshold values. Local overtemperatures in the interior of an SOFC stack may lead to an accelerated degradation of the stack, going along with a reduced efficiency. In the worst case, overtemperatures may even lead to the destruction of the SOFC. Due to the fact that temperature measurements in the interior of the SOFC should be restricted to a minimal amount of sensors (usually thermocouples), observer approaches can serve as software sensors in order to estimate the unmeasured temperatures and to detect possibly critical values in a model-based way.

Classical state observers provide point-valued estimates for all state variables of a dynamic system. In practice, such point values are only enough if the measured data are determined precisely and if all system parameters are accurately known. Concerning SOFC stacks, both prerequisites are commonly not fulfilled. On the one hand, measurement tolerances in the order of several Kelvin are typical for the thermocouples in industrially manufactured SOFC modules. On the other hand, also system parameters are subject to quite large uncertainty, partially stemming from the fact that nonlinear system models are embedded into quasi-linear state-space representations with a corresponding polytopic model of uncertainty that can be used for both guaranteed stabilizing control and observer design. Besides the set-valued estimation framework that is in the focus of this paper, also stochastic filtering techniques can be employed if appropriate probability density functions are available for the description of measurement noise and for the uncertainty in the dynamic process model.

In this paper, however, an interval-based state observer approach [5] is derived for the thermal subsystem of an SOFC stack. It is based on a finite volume modeling approach that produces an approximation of the temperature field in the interior of the SOFC stack in up to three space coordinates. A summary of this model, developed in [6] and the references therein, is given in Sec. II. Sec. III provides an analysis of structural system properties of this finite volume model with respect to its asymptotic stability and cooperativity. Both system properties can be verified if the (uncertain) system matrix in a quasi-linear state-space representation can be ensured to be simultaneously Hurwitz (ensuring asymptotic stability) and Metzler (guaranteeing cooperativity in the sense of monotonicity of the state trajectories wrt. the initial conditions). In Sec. IV, a state observer is designed which preserves both of these system properties and, therefore, allows for estimating interval bounds of all state variables. Experimental state estimation results are presented in Sec. V for a test rig available at the Chair of Mechatronics at the University of Rostock. Finally, conclusions and an outlook on future work are given in Sec. VI.

II. Control-Oriented Modeling of High-Temperature Fuel Cell Stacks

Mathematical models for the thermal behavior of SOFC systems consist of two fundamental components. Firstly, the dynamics of the stack module itself and, secondly, the

[1]Chair of Mechatronics, University of Rostock, Justus-von-Liebig-Weg 6, D-18059 Rostock, Germany {Andreas.Rauh, Julia.Kersten, Harald.Aschemann}@uni-rostock.de

lag behavior of anode and cathode gas preheaters with corresponding mass flow controllers have to be described to obtain sufficiently accurate representations for the internal temperature of the SOFC stack [6], cf. Fig. 1. Accurate, physically-oriented models for SOFC stacks are given by nonlinear partial differential equations [7], [8]. However, if control and real-time capable state estimation are concerned, finite-dimensional sets of ordinary differential equations (ODEs) are commonly preferred. These ODEs result from early lumping semi-discretization approaches. Starting from a balance of the internal energy over finitely large space domains, finite volume models can be obtained in which the stack temperature is approximated by piecewise homogeneous values in each volume element.

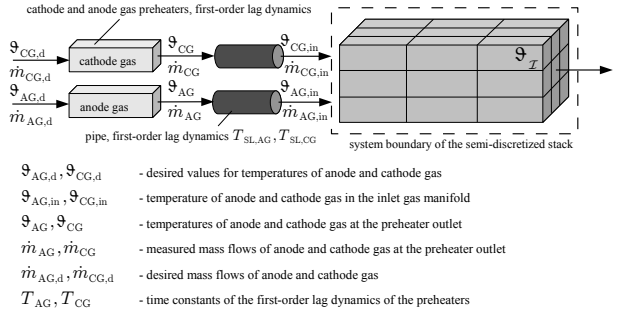

Fig. 1. Semi-discretization of the fuel cell stack module with gas preheaters according to [6] for a parallel flow configuration of anode and cathode gas.

Possible degrees of resolution of such models range from the treatment of the complete stack as a single volume element (reasonable for the design of controllers during the heating phase from the ambient temperature to a certain operating point), the discretization along the direction of mass flow if both the anode and cathode gas are supplied in parallel or anti-parallel directions, and to discretizations in two or three space coordinates to detect hot spot locations in a reliable way. In previous work, these models were already used for the design of feedback controllers which comprise both, interval-based predictive techniques and variable-structure approaches [9]–[12]. As shown in [12], all of these controllers rely on real-time estimates of the state variables, i.e., the previously mentioned piecewise homogeneous temperatures in the finite volume model. So far, point-valued estimation approaches were used for this purpose, which were a-posteriori extended by (heuristically chosen) interval bounds to include all possible operating points. Such interval extensions were also used in the algebraic derivative estimator presented in [12], which is necessary for the implementation of controllers that make use of a system representation in Brunovsky controller canonical form.

A. Modeling of the Thermal Behavior of the SOFC Stack

For the design of the interval-based state estimation scheme presented in this paper, a spatial semi-discretization of the complete SOFC stack is performed. For this purpose, the SOFC stack (given by the cuboid in Fig. 2) with the lengths L_L, L_M, and L_N of its corresponding perpendicular edges is subdivided into $n_x = L \cdot M \cdot N$ equally sized elements. For this type of homogeneous semi-discretization according to Fig. 2, each sub-cuboid has the edge lengths $l_L = \frac{L_L}{L}$, $l_M = \frac{L_M}{M}$, and $l_N = \frac{L_N}{N}$.

Based on [6] and [13], ODEs for the temperature in each finite volume element $\mathcal{I} := (i,j,k) \in \{(1,1,1),\ldots,(L,M,N)\}$, can be derived by local balance equations considering the following types of heat flows:

- HT: heat transfer due to heat conduction and convection (as a linearized model for heat radiation),
- G: enthalpy flows of the supplied gases, where χ in Fig. 2 denotes all relevant gas fractions,
- R: exothermic reaction enthalpy, and
- EL: Ohmic losses due to electric currents $I_{\mathcal{I}}$.

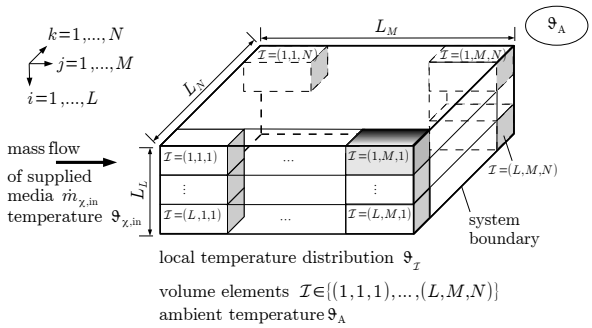

Fig. 2. Spatial semi-discretization of the fuel cell stack module.

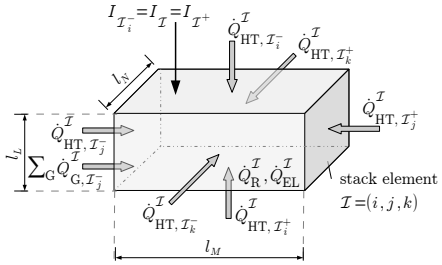

Fig. 3. Local energy balance of the semi-discretized fuel cell stack module.

As already mentioned, the following finite volume model is based on the assumption that all temperatures (and other dynamic variables such as mass flows and electric currents in extended system models) are homogeneously distributed in each volume element $\mathcal{I}$. For this reason, integral energy balances are formulated for all $\mathcal{I} := (i,j,k) \in \{(1,1,1),\ldots,(L,M,N)\}$. As far as the thermal behavior is concerned[1], the before-mentioned energy balances (cf. [3], [4]) lead to the ODEs

$$\dot{\vartheta}_{\mathcal{I}} = \frac{1}{c_{\mathcal{I}} m_{\mathcal{I}}} \left(\dot{Q}^{\mathcal{I}}_{\mathrm{HT}} + \sum_{\mathrm{G} \in \{\mathrm{AG,CG}\}} \dot{Q}^{\mathcal{I}}_{\mathrm{G},\mathcal{I}_j^-} + \dot{Q}^{\mathcal{I}}_{\mathrm{EL}} + \dot{Q}^{\mathcal{I}}_{\mathrm{R}} \right) \tag{1}$$

for the temperature $\vartheta_{\mathcal{I}} := \vartheta_{\mathcal{I}}(t)$ in each volume element $\mathcal{I}$ with the heat transfer expression

$$\begin{aligned} \dot{Q}^{\mathcal{I}}_{\mathrm{HT}} = \dot{Q}^{\mathcal{I}}_{\mathrm{HT},\mathcal{I}_i^-} + \dot{Q}^{\mathcal{I}}_{\mathrm{HT},\mathcal{I}_i^+} + \dot{Q}^{\mathcal{I}}_{\mathrm{HT},\mathcal{I}_j^-} + \\ \dot{Q}^{\mathcal{I}}_{\mathrm{HT},\mathcal{I}_j^+} + \dot{Q}^{\mathcal{I}}_{\mathrm{HT},\mathcal{I}_k^-} + \dot{Q}^{\mathcal{I}}_{\mathrm{HT},\mathcal{I}_k^+} \end{aligned} \tag{2}$$

[1]For a detailed description of fluidic properties of the SOFC stack, the reader is referred to [6].

and the total gas enthalpy flow $\sum_{\mathrm{G}} \dot{Q}^{\mathcal{I}}_{\mathrm{G},\mathcal{I}_j^-}$, $\mathrm{G} \in \{\mathrm{AG}, \mathrm{CG}\}$, for the anode gas (AG) and the cathode gas (CG) with the index convention $\mathcal{I}_i^- := (i-1, j, k)$, $\mathcal{I}_i^+ := (i+1, j, k)$, $\mathcal{I}_j^- := (i, j-1, k)$, $\mathcal{I}_j^+ := (i, j+1, k)$, $\mathcal{I}_k^- := (i, j, k-1)$, $\mathcal{I}_k^+ := (i, j, k+1)$. Here, $\vartheta_{\mathcal{I}_i^-}$ and $\vartheta_{\mathcal{I}_i^+}$ denote internal stack temperatures for $i \geq 2$ and $i \leq L-1$, $\vartheta_{\mathcal{I}_j^-}$ and $\vartheta_{\mathcal{I}_j^+}$ with $j \geq 2$ and $j \leq M-1$, as well as for $\vartheta_{\mathcal{I}_k^-}$ and $\vartheta_{\mathcal{I}_k^+}$ with $k \geq 2$ and $k \leq N-1$. For all other possible index values of i, j, and k, the values of $\vartheta_{\mathcal{I}_i^-}$, $\vartheta_{\mathcal{I}_i^+}$, $\vartheta_{\mathcal{I}_j^-}$, $\vartheta_{\mathcal{I}_j^+}$, $\vartheta_{\mathcal{I}_k^-}$, or $\vartheta_{\mathcal{I}_k^+}$ are equal to the ambient temperature $\vartheta_{\mathrm{A}} = \mathrm{const.}$

In addition to the heat transfer and enthalpy terms above, $\dot{Q}^{\mathcal{I}}_{\mathrm{EL}}$ and $\dot{Q}^{\mathcal{I}}_{\mathrm{R}}$ characterize Ohmic losses and exothermic heat production in the element $\mathcal{I}$ due to the reaction of hydrogen and oxygen. The remaining parameters in (1) are the specific heat capacity $c_{\mathcal{I}}$ and the mass $m_{\mathcal{I}}$ of the stack segment $\mathcal{I}$.

1) Heat Conduction, Convection and Radiation: Independent of whether electrochemical reactions take place in the interior of the SOFC stack, internal heat exchange between neighboring elements as well as heat exchange to the ambient medium according to Fig. 3 are fundamental influence factors for the energy balance in each finite volume element $\mathcal{I}$.

These heat transfer phenomena summarized in (2) are described by the expression

$$\dot{Q}^{\mathcal{I}}_{\mathrm{HT},\mathcal{J}} = \beta^{\mathcal{I}}_{\mathcal{J}} \cdot (\vartheta_{\mathcal{J}} - \vartheta_{\mathcal{I}}) \,, \; \mathcal{J} \in \{\mathcal{I}_i^-, \mathcal{I}_i^+, \mathcal{I}_j^-, \mathcal{I}_j^+, \mathcal{I}_k^-, \mathcal{I}_k^+\} \tag{3}$$

with the parameters

$$\beta^{\mathcal{I}}_{\mathcal{J}} = \begin{cases} \lambda^{(i)} \cdot \frac{l_N l_M}{l_L} & \text{for } \; \mathcal{J} = \mathcal{I}_i^-, \; i \geq 2 \\ & \text{or } \; \mathcal{J} = \mathcal{I}_i^+, \; i \leq L-1 \\ \lambda^{(j)} \cdot \frac{l_L l_N}{l_M} & \text{for } \; \mathcal{J} = \mathcal{I}_j^-, \; j \geq 2 \\ & \text{or } \; \mathcal{J} = \mathcal{I}_j^+, \; j \leq M-1 \\ \lambda^{(k)} \cdot \frac{l_L l_M}{l_N} & \text{for } \; \mathcal{J} = \mathcal{I}_k^-, \; k \geq 2 \\ & \text{or } \; \mathcal{J} = \mathcal{I}_k^+, \; k \leq N-1 \end{cases} \tag{4}$$

for heat conduction over each surface of the finite volume element $\mathcal{I}$ that is not in direct contact with the external insulation of the SOFC stack.

For each boundary surface, the heat transfer expression (3) represents convective heat transfer with the parameters

$$\beta^{\mathcal{I}}_{\mathcal{J}} = \begin{cases} \alpha^{(i)} \cdot l_N l_M & \text{for } \; \mathcal{J} = \mathcal{I}_i^-, \; i = 1 \\ & \text{or } \; \mathcal{J} = \mathcal{I}_i^+, \; i = L \\ \alpha^{(j)} \cdot l_L l_N & \text{for } \; \mathcal{J} = \mathcal{I}_j^-, \; j = 1 \\ & \text{or } \; \mathcal{J} = \mathcal{I}_j^+, \; j = M \\ \alpha^{(k)} \cdot l_L l_M & \text{for } \; \mathcal{J} = \mathcal{I}_k^-, \; k = 1 \\ & \text{or } \; \mathcal{J} = \mathcal{I}_k^+, \; k = N \; . \end{cases} \tag{5}$$

Nonlinear heat radiation processes across the system boundary are included in this model in a locally linearized form. This assumption is admissible because of the typical use of highly efficient insulating materials separating the hot inside of the SOFC stack from the ambiance.

In Eqs. (4) and (5), the heat conduction coefficients $\lambda^{(i)}$, $\lambda^{(j)}$, $\lambda^{(k)}$ as well as the convective heat transfer coefficients $\alpha^{(i)}$, $\alpha^{(j)}$, $\alpha^{(k)}$ need to be identified offline from measured data. Note that the simplifications $\lambda = \lambda^{(i)} = \lambda^{(j)} = \lambda^{(k)}$ and $\alpha = \alpha^{(i)} = \alpha^{(j)} = \alpha^{(k)}$ hold in good accuracy.

2) Enthalpy Flows of the Anode and Cathode Gas: The second influence factor on the thermal energy of the element $\mathcal{I}$ is the enthalpy flow $\sum_{\mathrm{G}} \dot{Q}^{\mathcal{I}}_{\mathrm{G},\mathcal{I}_j^-}$ from segment $\mathcal{I}_j^-$ to $\mathcal{I}$. It is composed of all constituents of the anode and cathode gases under the assumption that mass transport takes place only along the j-th coordinate (corresponding to an operation of the SOFC stack with parallel media supply) with

$$\sum_{\mathrm{G}} \dot{Q}^{\mathcal{I}}_{\mathrm{G},\mathcal{I}_j^-} := \sum_{\mathrm{G} \in \{\mathrm{AG},\mathrm{CG}\}} \dot{Q}^{\mathcal{I}}_{\mathrm{G},\mathcal{I}_j^-} = \dot{Q}^{\mathcal{I}}_{\mathrm{AG},\mathcal{I}_j^-} + \dot{Q}^{\mathcal{I}}_{\mathrm{CG},\mathcal{I}_j^-} \; . \tag{6}$$

In (6),

$$\dot{Q}^{\mathcal{I}}_{\mathrm{G},\mathcal{I}_j^-} = C_{\mathrm{G},\mathcal{I}}(\vartheta_{\mathcal{I}}, t) \cdot \Delta\vartheta^{\mathcal{I}}_{\mathrm{G},\mathcal{I}_j^-} \; , \quad \mathrm{G} \in \{\mathrm{AG}, \mathrm{CG}\} \; , \tag{7}$$

represents the enthalpy flows of the anode gas (AG) and the cathode gas (CG). The relevant temperature differences in (7) in the direction of the gas mass flow are defined by

$$\Delta\vartheta^{\mathcal{I}}_{\mathrm{G},\mathcal{I}_j^-} = \begin{cases} \vartheta_{\mathrm{G,in}} - \vartheta_{(i,1,k)} & \text{for } \; j = 1 \\ \vartheta_{\mathcal{I}_j^-} - \vartheta_{\mathcal{I}} & \text{for } \; j \in \{2, \ldots, M\} \; . \end{cases} \tag{8}$$

For the inlet gas manifold segment $j = 1$, the gas temperatures $\vartheta_{\mathrm{AG,in}}$ and $\vartheta_{\mathrm{CG,in}}$ in (8) correspond to the outlet temperatures of both gas preheaters in Fig. 1.

Moreover, the anode gas ($\mathrm{G} = \mathrm{AG}$) heat capacity

$$C_{\mathrm{AG},\mathcal{I}}(\vartheta_{\mathcal{I}}, t) = \sum_{\zeta \in \{\mathrm{H_2},\mathrm{N_2},\mathrm{H_2O}\}} c_{\zeta}(\vartheta_{\mathcal{I}}) \cdot \dot{m}_{\zeta}^{\mathcal{I}_j^-} \tag{9}$$

depends on the temperature $\vartheta_{\mathcal{I}}$ and on the local mass flows $\dot{m}_{\zeta}^{\mathcal{I}_j^-}$, $\zeta \in \{\mathrm{H_2}, \mathrm{N_2}, \mathrm{H_2O}\}$, of each fraction of the gas mixture. This holds analogously for the cathode gas ($\mathrm{G} = \mathrm{CG}$), where the heat capacity is given by

$$C_{\mathrm{CG},\mathcal{I}}(\vartheta_{\mathcal{I}}, t) \; = \; c_{\mathrm{CG}}(\vartheta_{\mathcal{I}}) \cdot \dot{m}_{\mathrm{CG}}^{\mathcal{I}_j^-} \; , \tag{10}$$

with the corresponding cathode gas mass flow $\dot{m}_{\mathrm{CG}}^{\mathcal{I}_j^-}(t)$ into the element $\mathcal{I}$. For both (9) and (10), it can be assumed that the temperatures of the gases are equal to the temperature of the $\mathcal{I}$-th volume element in the interior of the SOFC stack. This is a sufficiently accurate approximation due to the small size of the gas channels in the interior of the SOFC stack.

In (9) and (10), the specific heat capacities

$$c_{\chi}(\vartheta_{\mathcal{I}}) = \sum_{\nu=0}^{2} \gamma_{\chi,\nu} \cdot \vartheta_{\mathcal{I}}^{\nu} > 0 \tag{11}$$

are defined for each gas fraction $\chi \in \{\mathrm{H_2}, \mathrm{N_2}, \mathrm{H_2O}, \mathrm{CG}\}$ by temperature-dependent second-order polynomials with experimentally identified coefficients $\gamma_{\chi,\nu}$ [6].

3) Exothermic Reaction Enthalpy and Ohmic Losses: For non-vanishing electric currents of the SOFC, heat is produced in the interior of the stack module, on the one hand, due to the exothermic reaction between hydrogen and oxygen ($\dot{Q}^{\mathcal{I}}_{\mathrm{R}}$) and, on the other hand, due to Ohmic losses ($\dot{Q}^{\mathcal{I}}_{\mathrm{EL}}$).

Because both phenomena become relevant as soon as hydrogen is provided to the stack module at high-temperature

operating points, the local molar flow of consumed hydrogen $\Delta\dot{m}^{\mathcal{I}}_{\mathrm{H}_2}/M_{\mathrm{H}_2}$ needs to be balanced with the supplied gas mass flows and the produced mass flow of water vapor if the fluidic stack behavior is described. For a pure thermal modeling, the corresponding heat flows are treated subsequently as disturbances that become active as soon as the mass flow of hydrogen is not zero. Then, the exothermic reaction heat flow is given by

$$\dot{Q}^{\mathcal{I}}_{\mathrm{R}} = -\frac{H_{\mathrm{R}}(\vartheta_{\mathcal{I}}) \cdot \Delta\dot{m}^{\mathcal{I}}_{\mathrm{H}_2}}{M_{\mathrm{H}_2}} = \frac{H_{\mathrm{R}}(\vartheta_{\mathcal{I}}) \cdot I_{\mathcal{I}}}{z \cdot F} \quad , \tag{12}$$

where

$$H_{\mathrm{R}}(\vartheta_{\mathcal{I}}) = \sum_{\nu=0}^{2} \gamma_{\mathrm{H_R},\nu} \cdot \vartheta^{\nu}_{\mathcal{I}} \tag{13}$$

denotes the polynomial approximation of the temperature-dependent molar reaction enthalpy with experimentally identified parameters $\gamma_{\mathrm{H_R},\nu}$. Moreover, $z = 4$ is the number of electrons involved in the electrochemical reaction, F the Faraday constant, and $I_{\mathcal{I}}$ the local electric current in the volume element $\mathcal{I}$. Then, heat flows

$$\dot{Q}^{\mathcal{I}}_{\mathrm{EL}} = R_{\mathrm{EL},\mathcal{I}} \cdot I^2_{\mathcal{I}} \tag{14}$$

due to Ohmic losses result from the current $I_{\mathcal{I}}$ through the interior of the stack with the non-zero resistance R_{EL}, $R_{\mathrm{EL},\mathcal{I}} = \frac{M \cdot N}{L} \cdot R_{\mathrm{EL}}$.

4) Reliable Parameterization of the System Model and Interval Representation of Uncertain State-Dependent Characteristics: As mentioned above, the temperature dependency of the (specific) heat capacities of all constituents of the anode and cathode gas as well as the temperature dependency of the reaction enthalpy of hydrogen are described in terms of second-order polynomials (11) and (13), respectively, which both depend on the element temperatures $\vartheta_{\mathcal{I}}$. To obtain an accurate system model, the parameters of these characteristics as well as the coefficients for heat conduction and heat convection have been identified in previous work by using either local or global optimization techniques [14]–[16]. For that purpose, temperature measurements are required at selected positions in the interior and at the boundary of the SOFC stack module. In such a way, it is possible to determine interval bounds for the parameters $\mathbf{p}$ of the nonlinear state-space representation

$$\dot{\mathbf{x}} = \mathbf{f}\left(\mathbf{x}, \mathbf{p}, \mathbf{u}\right) \tag{15}$$

for the temperature distribution in the interior of the SOFC stack. In (15), the state vector is given by

$$\mathbf{x} = \begin{bmatrix} \vartheta_{(1,1,1)} & \dots & \vartheta_{(L,M,N)} \end{bmatrix}^T \in \mathbb{R}^{n_x} \tag{16}$$

with $n_x = L \cdot M \cdot N$, where $\mathbf{u}$ summarizes all control inputs and external influences such as changes of the ambient temperature. Further refinements of this ODE model, accounting also for the preheater dynamics, were published in [6], [12].

Due to the fact that all local mass flows $\dot{m}^{\mathcal{I}_j}_{\chi}$, $\chi \in \{\mathrm{H}_2, \mathrm{N}_2, \mathrm{H}_2\mathrm{O}, \mathrm{CG}\}$, are strictly non-negative and that the parameters in (11) and (13) have to be chosen such that $c_{\chi}(\vartheta_{\mathcal{I}}) > 0$ is satisfied for the worst-case range $\vartheta_{\mathcal{I}} \in \left[\underline{\Theta}\,;\,\overline{\Theta}\right]$ of all possible SOFC stack temperatures, it is not only guaranteed that the uncertain parameters $\mathbf{p}$ can be bounded within an interval box $[\mathbf{p}] = \left[\underline{\mathbf{p}}\,;\,\overline{\mathbf{p}}\right]$, where $\underline{p}_i \leq p_i \leq \overline{p}_i$ holds for each vector component $i = \{1, \dots, n_{\mathrm{p}}\}$, $\mathbf{p} \in \mathbb{R}^{n_{\mathrm{P}}}$, but also that the anode and cathode gas heat capacities are restricted by the intervals

$$C_{\mathrm{AG},\mathcal{I}}(\vartheta_{\mathcal{I}}, t) \in \left[\underline{C}_{\mathrm{AG},\mathcal{I}}\,;\,\overline{C}_{\mathrm{AG},\mathcal{I}}\right] \quad , \quad \underline{C}_{\mathrm{AG},\mathcal{I}} > 0 \tag{17}$$

as well as

$$C_{\mathrm{CG},\mathcal{I}}(\vartheta_{\mathcal{I}}, t) \in \left[\underline{C}_{\mathrm{CG},\mathcal{I}}\,;\,\overline{C}_{\mathrm{CG},\mathcal{I}}\right] \quad , \quad \underline{C}_{\mathrm{CG},\mathcal{I}} > 0 \tag{18}$$

for all possible operating points of the SOFC stack. These bounds will be used in the following sections for the structural analysis of the system model as well as for the design of an interval observer that is capable of estimating those cell temperatures that are compatible with measurements $\mathbf{y}_{\mathrm{m}}$ characterized by interval-valued tolerances $[-\Delta\mathbf{y}_{\mathrm{m}}\,;\,\Delta\mathbf{y}_{\mathrm{m}}]$ according to $[\mathbf{y}_{\mathrm{m}}] = \mathbf{y}_{\mathrm{m}} + [-\Delta\mathbf{y}_{\mathrm{m}}\,;\,\Delta\mathbf{y}_{\mathrm{m}}]$.

In what follows, it is assumed that the measured temperatures are given by $\mathbf{y} = \mathbf{C}\mathbf{x}$, where the output matrix $\mathbf{C}$ is zero except for a single entry equal to one in each row which specifies the correspondingly measured temperature value of the finite volume model.

As soon as element-wise defined interval bounds $\mathbf{x} \in [\mathbf{v}\,;\,\mathbf{w}]$ are known for each state variable, corresponding bounds $\mathbf{y} = \mathbf{C}\mathbf{x} \in [\mathbf{y}] = [\mathbf{C}\mathbf{v}\,;\,\mathbf{C}\mathbf{w}]$ can also be determined for each of the system outputs. This property is exploited in Sec. IV in which an interval-based state observer is designed which makes use of the cooperativity property [17] of the system model discussed in the following section.

III. Cooperativity and Stability Analysis of the System Model

Due to the structure of the system model (15), it is possible to rewrite the nonlinear state equations into a quasi-linear state-space representation

$$\dot{\mathbf{x}} = \mathbf{A}\left(\mathbf{x}, \mathbf{p}\right) \cdot \mathbf{x} + \mathbf{B}\left(\mathbf{x}, \mathbf{p}\right) \cdot \mathbf{u} \tag{19}$$

in which the system and input matrices $\mathbf{A}\left(\mathbf{x}, \mathbf{p}\right)$ and $\mathbf{B}\left(\mathbf{x}, \mathbf{p}\right)$ depend on the state vector (16) as well as on the interval parameters $[\mathbf{p}]$. Independent of the dimension n_x of the state vector, the system matrix $\mathbf{A}\left(\mathbf{x}, \mathbf{p}\right)$ is structured such that its diagonal elements are strictly negative and that off-diagonal elements are either zero or strictly positive. Hence, it is guaranteed that the system matrix is Metzler, corresponding to a sufficient condition for cooperativity of the state equations. Moreover, all entries in $\mathbf{B}\left(\mathbf{x}, \mathbf{p}\right)$ are also guaranteed to be non-negative for all physically reasonable operating points. Taking further into account that all state variables are strictly positive for all points of time (corresponding to temperature values measured in Kelvin) and that also all components of $\mathbf{u}$ are non-negative, the system model is monotonic in the initial conditions and all state variables stay in the positive orthant for all points of time $t \geq 0$. This property of positivity is exploited together with the following

stability property to design an interval observer that allows for computing worst-case lower and upper state boundaries despite bounded measurement tolerances.

The stability properties are analyzed subsequently for the special case $L = N = 1$ with $M = 3$. However, these properties hold analogously for any other choice $L, M, N \geq 1$ in the semi-discretization approach.

For the discretization of the SOFC stack into three elements in the direction of the gas mass flow, the system and input matrices have the following form

$$\mathbf{A}\left(\mathbf{x},\mathbf{p}\right) = \begin{bmatrix} a_{11} & a_{12} & 0 \\ a_{21} & a_{22} & a_{23} \\ 0 & a_{32} & a_{33} \end{bmatrix} \tag{20}$$

and

$$\mathbf{B}\left(\mathbf{x},\mathbf{p}\right) = \begin{bmatrix} b_{11} & b_{12} & b_{13} & b_{14} \\ b_{21} & 0 & 0 & b_{24} \\ b_{31} & 0 & 0 & b_{34} \end{bmatrix} \ , \tag{21}$$

where the state and input vectors are defined by

$$\mathbf{x} = \begin{bmatrix} \vartheta_{(1,1,1)} & \vartheta_{(1,2,1)} & \vartheta_{(1,3,1)} \end{bmatrix}^T \tag{22}$$

and

$$\mathbf{u} = \begin{bmatrix} \vartheta_{\mathrm{A}} & \vartheta_{\mathrm{AG,in}} & \vartheta_{\mathrm{CG,in}} & \frac{1}{3}I \end{bmatrix}^T \tag{23}$$

with $I_{(1,1,1)} = I_{(1,2,1)} = I_{(1,3,1)} = \frac{1}{3}I$.

The non-zero entries of the matrix (20) are given by

$$\begin{aligned}
a_{11} &= \frac{1}{c_{\mathcal{I}} m_{\mathcal{I}}} \cdot \Bigg(-\lambda \frac{l_L l_N}{l_M} - \alpha \left(2 l_N l_M + l_L l_N + 2 l_L l_M\right) \\
&\quad - C_{\mathrm{AG},(1,1,1)}(\vartheta_{(1,1,1)}, t) - C_{\mathrm{CG},(1,1,1)}(\vartheta_{(1,1,1)}, t) \Bigg) \\
a_{12} &= \frac{1}{c_{\mathcal{I}} m_{\mathcal{I}}} \cdot \lambda \frac{l_L l_N}{l_M} \\
a_{21} &= \frac{1}{c_{\mathcal{I}} m_{\mathcal{I}}} \cdot \Bigg(\lambda \frac{l_L l_N}{l_M} + C_{\mathrm{AG},(1,2,1)}(\vartheta_{(1,2,1)}, t) \\
&\quad + C_{\mathrm{CG},(1,2,1)}(\vartheta_{(1,2,1)}, t) \Bigg) \\
a_{22} &= \frac{1}{c_{\mathcal{I}} m_{\mathcal{I}}} \cdot \Bigg(-2\lambda \frac{l_L l_N}{l_M} - 2\alpha \left(l_N l_M + l_L l_M\right) \\
&\quad - C_{\mathrm{AG},(1,2,1)}(\vartheta_{(1,2,1)}, t) - C_{\mathrm{CG},(1,2,1)}(\vartheta_{(1,2,1)}, t) \Bigg) \\
a_{23} &= \frac{1}{c_{\mathcal{I}} m_{\mathcal{I}}} \cdot \lambda \frac{l_L l_N}{l_M} \\
a_{32} &= \frac{1}{c_{\mathcal{I}} m_{\mathcal{I}}} \cdot \Bigg(\lambda \frac{l_L l_N}{l_M} + C_{\mathrm{AG},(1,3,1)}(\vartheta_{(1,3,1)}, t) \\
&\quad + C_{\mathrm{CG},(1,3,1)}(\vartheta_{(1,3,1)}, t) \Bigg) \\
a_{33} &= \frac{1}{c_{\mathcal{I}} m_{\mathcal{I}}} \cdot \Bigg(-\lambda \frac{l_L l_N}{l_M} - \alpha \left(2 l_N l_M + l_L l_N + 2 l_L l_M\right) \\
&\quad - C_{\mathrm{AG},(1,3,1)}(\vartheta_{(1,3,1)}, t) - C_{\mathrm{CG},(1,3,1)}(\vartheta_{(1,3,1)}, t) \Bigg) \ .
\end{aligned}$$

Analogously, the non-zero matrix entries of (21) are

$$\begin{aligned}
b_{11} &= \frac{1}{c_{\mathcal{I}} m_{\mathcal{I}}} \cdot \alpha \left(2 l_N l_M + l_L l_N + 2 l_L l_M\right) \\
b_{12} &= \frac{1}{c_{\mathcal{I}} m_{\mathcal{I}}} \cdot C_{\mathrm{AG},(1,1,1)}(\vartheta_{(1,1,1)}, t) \\
b_{13} &= \frac{1}{c_{\mathcal{I}} m_{\mathcal{I}}} \cdot C_{\mathrm{CG},(1,1,1)}(\vartheta_{(1,1,1)}, t) \\
b_{14} &= \frac{1}{c_{\mathcal{I}} m_{\mathcal{I}}} \cdot \left(\frac{H_{\mathrm{R}}(\vartheta_{(1,1,1)})}{z \cdot F} + 3 R_{\mathrm{EL}} \cdot I_{(1,1,1)} \right) \\
b_{21} &= \frac{1}{c_{\mathcal{I}} m_{\mathcal{I}}} \cdot \alpha \left(2 l_N l_M + 2 l_L l_M\right) \\
b_{24} &= \frac{1}{c_{\mathcal{I}} m_{\mathcal{I}}} \cdot \left(\frac{H_{\mathrm{R}}(\vartheta_{(1,2,1)})}{z \cdot F} + 3 R_{\mathrm{EL}} \cdot I_{(1,2,1)} \right) \\
b_{31} &= \frac{1}{c_{\mathcal{I}} m_{\mathcal{I}}} \cdot \alpha \left(2 l_N l_M + l_L l_N + 2 l_L l_M\right) \\
b_{34} &= \frac{1}{c_{\mathcal{I}} m_{\mathcal{I}}} \cdot \left(\frac{H_{\mathrm{R}}(\vartheta_{(1,3,1)})}{z \cdot F} + 3 R_{\mathrm{EL}} \cdot I_{(1,3,1)} \right) \ .
\end{aligned}$$

Due to the fact that the only negative matrix entries are $a_{11} < 0$, $a_{22} < 0$, and $a_{33} < 0$, the above-mentioned Metzler property is obviously satisfied. Moreover, the plant model is guaranteed to be asymptotically stable. This can be proven by computing upper bounds for the real parts of all eigenvalues λ_i by exploiting the Gershgorin circle theorem [18] according to

$$\begin{aligned}
\Re\{\lambda_i\} &\leq a_{ii} + \sum_{j=1, j\neq i}^{n_x=3} |a_{ij}| \\
&= \begin{cases}
\frac{1}{c_{\mathcal{I}} m_{\mathcal{I}}} \cdot \Big(-\alpha \left(2 l_N l_M + l_L l_N + 2 l_L l_M\right) \\
\quad -C_{\mathrm{AG},(1,1,1)}(\vartheta_{(1,1,1)}, t) \\
\quad -C_{\mathrm{CG},(1,1,1)}(\vartheta_{(1,1,1)}, t) \Big) < 0 & \text{for } i = 1 \\
\frac{-2\alpha}{c_{\mathcal{I}} m_{\mathcal{I}}} \cdot \left(l_N l_M + l_L l_M\right) < 0 & \text{for } i = 2 \\
\frac{-\alpha}{c_{\mathcal{I}} m_{\mathcal{I}}} \cdot \left(2 l_N l_M + l_L l_N + 2 l_L l_M\right) < 0 & \text{for } i = 3 \ .
\end{cases}
\end{aligned} \tag{24}$$

IV. Interval Observer Design

Taking into account that the inequalities $\underline{\mathbf{A}} \leq \mathbf{A}\left(\mathbf{x},\mathbf{p}\right) \leq \overline{\mathbf{A}}$ and $\mathbf{0} \leq \underline{\mathbf{B}} \leq \mathbf{B}\left(\mathbf{x},\mathbf{p}\right) \leq \overline{\mathbf{B}}$ hold in an element-wise manner, an interval observer [5] can be defined according to

$$\underline{\mathbf{A}}_{\mathrm{O}} \hat{\mathbf{v}} + \underline{\mathbf{B}} \mathbf{u} + \mathbf{H} \underline{\mathbf{y}}_{\mathrm{m}} \leq \dot{\hat{\mathbf{x}}} \leq \overline{\mathbf{A}}_{\mathrm{O}} \hat{\mathbf{w}} + \overline{\mathbf{B}} \mathbf{u} + \mathbf{H} \overline{\mathbf{y}}_{\mathrm{m}} \ . \tag{25}$$

Asymptotic stability of the error dynamics associated with the bounding systems on the left- and right-hand sides of (25) is guaranteed if $\underline{\mathbf{A}}_{\mathrm{O}}$ and $\overline{\mathbf{A}}_{\mathrm{O}}$ are defined as

$$\underline{\mathbf{A}}_{\mathrm{O}} = \underline{\mathbf{A}} - \mathbf{H}\mathbf{C} \quad \text{and} \quad \overline{\mathbf{A}}_{\mathrm{O}} = \overline{\mathbf{A}} - \mathbf{H}\mathbf{C} \tag{26}$$

with the observer gain matrix

$$\mathbf{H} = \kappa \mathbf{C}^T \quad \text{and} \quad \kappa > 0 \ . \tag{27}$$

Because the product $\mathbf{H}\mathbf{C} = \kappa \mathbf{C}^T \mathbf{C}$ yields a pure diagonal matrix with the elements 0 and $\kappa > 0$, it is guaranteed that both bounding systems in (25) remain cooperative (positive) and that the observer error dynamics is asymptotically stable. The proof of the latter property is straightforward by substituting both matrices in (26) for the corresponding matrix entries in (24). Due to the asymptotic stability and cooperativity of the observer error dynamics, the actual system states $\mathbf{x}$ are guaranteed to be included in the estimated interval vector according to $\mathbf{x} \in [\hat{\mathbf{x}}] := [\hat{\mathbf{v}} \ ; \ \hat{\mathbf{w}}]$ for the uncertain measurements $[\mathbf{y}_{\mathrm{m}}] = \mathbf{y}_{\mathrm{m}} + [-\Delta\mathbf{y}_{\mathrm{m}} \ ; \ \Delta\mathbf{y}_{\mathrm{m}}]$.

V. Experimental Validation: Estimation of the SOFC Temperature During the Heating Phase

Fig. 4 shows the lower and upper temperature bounds that have been computed by the interval-based observer introduced in the previous section for real measured data gathered during the heating phase of an SOFC stack module available at the Chair of Mechatronics at the University of Rostock with $L = N = 1$ and $M = 3$, cf. Sec. III. For the implementation of the observer with $\mathbf{C} = \begin{bmatrix} 0 & 0 & 1 \end{bmatrix}$, the parameter $\kappa = 1$ was chosen together with the measurement tolerance $\Delta y_\mathrm{m} = 15\,\mathrm{K}$ which corresponds to the same tolerance bound that was also considered in the global parameter identification routines discussed in [9]–[12] and the references therein. It can be seen clearly that the inequality $\hat{\mathbf{v}} < \hat{\mathbf{w}}$ holds for each component of the estimated state vectors. Moreover, the obtained bounds are significantly tighter than the ones that can be obtained by a predictor–corrector framework according to [19]. Note that the computational effort is also much smaller than for any predictor–corrector approach which inevitably needs to be implemented by an interval subdivision scheme with multiple evaluations of the complete set of state equations for interval domains of initial states, cf. [19].

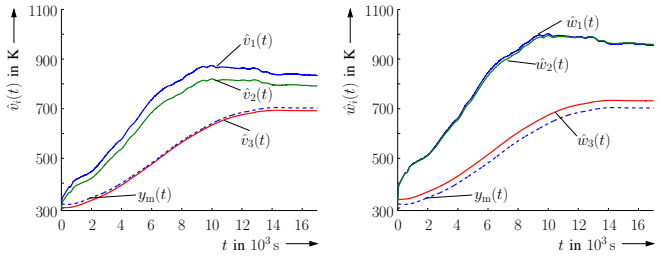

(a) Lower temperature bounds $\hat{v}_i$. (b) Upper temperature bounds $\hat{w}_i$.

Fig. 4. Estimated state boundaries (solid lines) and measured stack outlet temperature $y_\mathrm{m}(t)$ (dashed line).

VI. Conclusions and Outlook on Future Work

In this paper, finite volume models for SOFC stack modules were designed in such a way that they are structurally cooperative and asymptotically stable. These properties were exploited successfully for the design of an interval observer which allows for an efficient computation of lower and upper state boundaries despite uncertainty in the system matrices of quasi-linear state equations and interval tolerances of measured data. The suggested observer is readily applicable to be interfaced with robust control procedures such as sensitivity-based or variable-structure controllers [9], [19].

In future work, extensions of the observer approach will be developed which allow for a computationally efficient identification of the system model. So far, global optimization routines were used for this purpose which do not exploit the cooperativity properties of the system model. Because the lower and upper bounding systems in (25) are mutually independent, a parallelized evaluation of both bounding systems can be implemented in a straightforward manner.

References

[1] C. Stiller, "Design, Operation and Control Modelling of SOFC/GT Hybrid Systems," Ph.D. dissertation, University of Trondheim, 2006.

[2] C. Stiller, B. Thorud, O. Bolland, R. Kandepu, and L. Imsland, "Control Strategy for a Solid Oxide Fuel Cell and Gas Turbine Hybrid System," *Journal of Power Sources*, vol. 158, pp. 303–315, 2006.

[3] J. Pukrushpan, A. Stefanopoulou, and H. Peng, *Control of Fuel Cell Power Systems: Principles, Modeling, Analysis and Feedback Design*, 2nd ed. Berlin: Springer–Verlag, 2005.

[4] R. Bove and S. Ubertini, Eds., *Modeling Solid Oxide Fuel Cells*. Berlin: Springer–Verlag, 2008.

[5] D. Efimov, T. Rassi, S. Chebotarev, and A. Zolghadri, "Interval state observer for nonlinear time varying systems," *Automatica*, vol. 49, no. 1, pp. 200–205, 2013.

[6] A. Rauh, L. Senkel, J. Kersten, and H. Aschemann, "Reliable Control of High-Temperature Fuel Cell Systems using Interval-Based Sliding Mode Techniques," *IMA Journal of Mathematical Control and Information*, vol. 33, no. 2, pp. 457–484, 2016.

[7] B. Huang, Y. Qi, and A. Murshed, "Solid Oxide Fuel Cell: Perspective of Dynamic Modeling and Control," *Journal of Process Control*, vol. 21, no. 10, pp. 1426–1437, 2011.

[8] ——, *Dynamic Modeling and Predictive Control in Solid Oxide Fuel Cells: First Principle and Data-based Approaches*. Chichester, UK: John Wiley & Sons, 2013.

[9] A. Rauh, L. Senkel, and H. Aschemann, "Reliable Sliding Mode Approaches for the Temperature Control of Solid Oxide Fuel Cells with Input and Input Rate Constraints," in *Proceedings of 1st IFAC Conference on Modelling, Identification and Control of Nonlinear Systems, MICNON 2015*, St. Petersburg, Russia, 2015.

[10] ——, "Interval-Based Sliding Mode Control Design for Solid Oxide Fuel Cells with State and Actuator Constraints," *IEEE Transactions on Industrial Electronics*, vol. 62, no. 8, pp. 5208–5217, 2015.

[11] A. Rauh, L. Senkel, J. Kersten, and H. Aschemann, "Verified Stability Analysis for Interval-Based Sliding Mode and Predictive Control Procedures with Applications to High-Temperature Fuel Cell Systems," in *Proceedings of 9th IFAC Symposium on Nonlinear Control Systems*, Toulouse, France, 2013.

[12] A. Rauh and L. Senkel, "Interval Methods for Robust Sliding Mode Control Synthesis of High-Temperature Fuel Cells with State and Input Constraints," in *Variable-Structure Approaches: Analysis, Simulation, Robust Control and Estimation of Uncertain Dynamic Processes*, ser. Math. Eng., A. Rauh and L. Senkel, Eds. Springer–Verlag, 2016, pp. 53–85.

[13] A. Rauh, L. Senkel, and H. Aschemann, "Variable Structure Approaches for Temperature Control of Solid Oxide Fuel Cell Stacks," in *Proc. of 2nd Intl. Conference on Vulnerability and Risk Analysis and Management ICVRAM 2014*, Liverpool, UK, 2014.

[14] E. Auer, S. Kiel, and A. Rauh, "Verified Parameter Identification for Solid Oxide Fuel Cells," in *Proceedings of 5th International Conference on Reliable Engineering Computing*, Brno, Czech Repulic, 2012, pp. 41–55, http://rec2012.fce.vutbr.cz/documents/proceedings/REC2012_proceedings.pdf, accessed: May 29, 2017.

[15] A. Rauh, T. Dötschel, E. Auer, and H. Aschemann, "Interval Methods for Control-Oriented Modeling of the Thermal Behavior of High-Temperature Fuel Cell Stacks," in *Proceedings of 16th IFAC Symposium on System Identification SysID 2012*, Brussels, Belgium, 2012.

[16] L. Senkel, A. Rauh, and H. Aschemann, "Experimental Validation of a Sensitivity-Based Observer for Solid Oxide Fuel Cell Systems," in *Proceedings of IEEE International Conference on Methods and Models in Automation and Robotics MMAR 2013*, Miedzyzdroje, Poland, 2013.

[17] H. L. Smith, *Monotone Dynamical Systems: An Introduction to the Theory of Competitive and Cooperative Systems*. Mathematical Surveys and Monographs, American Mathematical Soc., 1995, vol. 41.

[18] A. Weinmann, *Uncertain Models and Robust Control*. Wien: Springer–Verlag, 1991.

[19] A. Rauh, L. Senkel, J. Kersten, and H. Aschemann, "Interval Methods for Sensitivity-Based Model-Predictive Control of Solid Oxide Fuel Cell Systems," in *Proceedings of the 15th GAMM-IMACS International Symposium on Scientific Computing, Computer Arithmetic, and Validated Numerics SCAN 2012*, vol. 19(4), Novosibirsk, Russia, 2014, pp. 361–384, special Issue of Reliable Computing, http://interval.louisiana.edu/reliable-computing-journal/volume-19/reliable-computing-19-pp-361-384.pdf.